On the Thermodynamics of Water Displacement from Binding Sites and its Contributions to Supramolecular and Biomolecular Affinity

Jeffry Setiadi[1,], Frank Biedermann[2*], Werner M. Nau[3*], Michael K. Gilson[1*]

1. Skaggs School of Pharmacy and Pharmaceutical Sciences, 9255 Pharmacy Lane, University of California San Diego, La Jolla, CA, 92093, USA
2. Institute of Nanotechnology (INT), Karlsruhe Institute of Technology (KIT), Hermann-von-Helmholtz Platz 1, 76344 Eggenstein-Leopoldshafen, Germany
3. School of Science, Constructor University, Campus Ring 1, 28759 Bremen, Germany

*wnau@constructor.university, frank.biedermann@kit.edu, mgilson@ucsd.edu

Abstract

The role of water displacement in noncovalent binding has been debated in the fields of supramolecular chemistry and drug design. We use molecular dynamics simulations of idealized host-guest systems to address the long-standing controversy of whether water is merely a bystander or an actual driver of noncovalent binding in aqueous solution. To isolate hydration effects, we consider a pseudo-hard-sphere guest binding to a series of cucurbit[8]uril-based host models whose energetic interactions with water vary widely. The computed free energy cost of displacing water from binding sites ranges from 0 to +37 kcal/mol, strongly influencing binding affinities. However, neither water density nor excess chemical potential reliably indicates the thermodynamic favorability of cavity water. These results support the concept that "unfavorable" binding site water contributes to high-affinity binding and resolve the paradox of stable but thermodynamically unfavorable cavity water. This work provides insights into the nature of the hydrophobic effect in molecular recognition and offers a framework for understanding water's role in binding across various host-guest and protein-ligand systems.

1 Introduction

Life is based on water as medium, and almost all key biological processes – such as the self-assembly of lipid bilayers, the folding of proteins, ligand-receptor and enzyme-substrate binding, and nucleic acid hybridization -- involve displacement of water from binding sites and interaction surfaces. However, it has remained a matter of vivid debate whether (and, if so, to what degree) the displacement of water molecules plays an active driving role in such processes. Even turning to the simplest model systems for these phenomena, namely macrocyclic hosts that bind hydrophobic guest molecules, has not resolved this question, but has, instead, escalated the controversy.
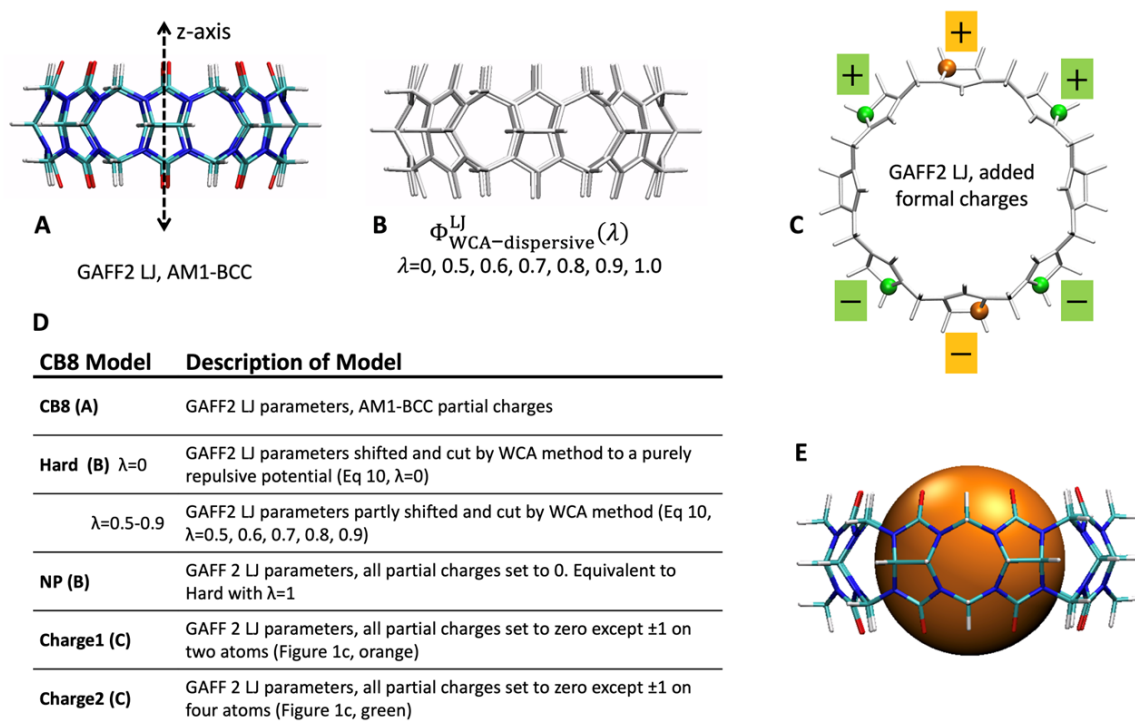
The binding of a guest molecule within the cavity of a macrocyclic host in water indisputably displaces, or releases, water from the binding site. Early studies of cyclodextrins suggested that the water in their nonpolar binding sites was "enthalpy-rich", "high-energy", or "energy-rich"[1–3], so that its displacement makes a favorable enthalpic contribution to the binding free energy. The idea that water in a concave, nonpolar cavity exists in a high enthalpy state appeared to contradict the traditional idea that the hydrophobic effect is entropy-driven[4], rather than enthalpy-driven, so Diederich coined the term "non-classical hydrophobic effect" for such cases[5,6]. Subsequent work recognized that water enclosed in a hydrophobic cleft could also be considerably lower in entropy than water at the surface of a convex hydrophobic solute. Consequently, its displacement makes a particularly favorable entropic contribution to binding[7]. In general, binding site water whose displacement favors binding, whether enthalpically, entropically, or both, may be termed "high free energy", "free energetically unfavorable"[8], "activated"[9,10], "frustrated"[11], "unstable", "xenophobic", "unhappy", or simply "unfavorable"[12].

This role of water displacement as a determinant of binding thermodynamics has been extensively studied in supramolecular chemistry, well beyond the cyclodextrin and cyclophane macrocycles where it originated[13–21]. For cucurbiturils, which stand out due to their ultrahigh affinity binding[22–25], the importance of thermodynamically unfavorable binding site water became apparent early[26,27] and stimulated early computational descriptions[28–30]. In addition, thermodynamic analysis of binding site water is now widely used in structure-based drug design[31–37], as ligands can gain affinity by displacing the water from protein subpockets where it is particularly unfavorable[34,35,38].

Although theoretical work on thermodynamic densities in fluids provides the foundation of these concepts[12,39], and they are well connected to the results of atomistic simulations[7,35,36,40–46], the idea that the displacement of cavity water contributes to binding has been challenged[47–49]. Critics argue that the chemical potential of water in a solution is uniform and not position-dependent, meaning there is nothing thermodynamically unique about water in a specific location, such as a binding cavity. This perspective, though, remains a topic of theoretical debate[12]. Dewetting, or drying, of cavities has been offered as an alternative viewpoint[50,51], but whether and how the "dried" nature of a cavity can drive binding remains unclear. In addition, a dried cavity is arguably only an extreme manifestation of high-energy water[52,53], so it should be possible to bring the two concepts into accordance.

Here, we elucidate the thermodynamic contributions of water displacement through computational analysis of idealized, aqueous host-guest systems specifically designed to address the issues raised above. We use molecular dynamics (MD) simulations to compute the binding free energy of a simple guest to a series of hosts that interact more or less favorably with water. At one extreme, water occupancy is so unfavorable that the binding site has dewetted. At the other extreme, water is tightly bound within a highly ionic host. We isolate the contributions of solvent to binding by using what is essentially a hard-sphere guest model that has negligible interactions with both the hosts and the solvent. In addition, the

series of host molecules include an essentially "hard" host so that we can compute the affinity of the host-guest system with near-zero host-guest, host-solvent, and guest-solvent interaction energies.

A GAFF2 LJ, AM1-BCC

B $\Phi^{LJ}_{WCA-dispersive}(\lambda)$
λ=0, 0.5, 0.6, 0.7, 0.8, 0.9, 1.0

C GAFF2 LJ, added formal charges

D

CB8 Model	Description of Model
CB8 (A)	GAFF2 LJ parameters, AM1-BCC partial charges
Hard (B) λ=0	GAFF2 LJ parameters shifted and cut by WCA method to a purely repulsive potential (Eq 10, λ=0)
λ=0.5-0.9	GAFF2 LJ parameters partly shifted and cut by WCA method (Eq 10, λ=0.5, 0.6, 0.7, 0.8, 0.9)
NP (B)	GAFF 2 LJ parameters, all partial charges set to 0. Equivalent to Hard with λ=1
Charge1 (C)	GAFF 2 LJ parameters, all partial charges set to zero except ±1 on two atoms (Figure 1c, orange)
Charge2 (C)	GAFF 2 LJ parameters, all partial charges set to zero except ±1 on four atoms (Figure 1c, green)

E

2   Methods

Figure 1. Models of the cucurbit[8]uril (CB8) host molecule studied here. All are treated as rigid. A) CB8 with full GAFF2 Lennard Jones (LJ) parameters and AM1-BCC partial charges. The axis of symmetry (z-axis) is labeled. B) No partial charges, LJ dispersive interactions scaled from $\lambda = 0$ (no dispersion interactions) to $\lambda = 1$ (full LJ) using Eq (13), and C) no partial charges except for $\pm 1e$ placed on one pair (orange) or two pairs (green) of equatorial carbon atoms. D) Table summarizing the model hosts and their names. E) CB8 with the 5 Å pseudo-hard sphere "guest" (orange) displacing all water molecules from the binding cavity.

2.1   Overview of model systems and calculations

We used molecular simulations of idealized host-guest systems in explicit water to isolate and study the contribution of water to binding thermodynamics. Any thermodynamic contribution to binding attributable to direct host-guest interactions is eliminated by using a pseudo-hard-sphere potential (PHSP) for the host-guest interaction. This accounts for sterics but has no attractive component (details below). We also treat the host and guest as rigid, i.e., without internal degrees of freedom, to avoid thermodynamic contributions to the binding free energies that result from conformational deformations and fluctuations. In addition, instead of computing the standard free energy of binding, which accounts for entropy changes due to changes in the distribution of the relative coordinates of the two molecules on binding[54], we compute the potential of mean force (PMF) – essentially the free energy -- as the guest is moved from outside the host to inside the host along the host's axis of symmetry (z-axis, Figure 1A). The size of the spherical guest is set to be small enough that it does not clash sterically with the host when moved along the z-axis. Therefore, the PMF will be flat if there is no solvent-mediated interaction between the host and guest, such as if the calculation were done *in vacuo*. If displacing solvent from the two molecules (i.e., the host and guest) on binding is favorable, then the PMF will fall as the guest enters the

host. Conversely, if displacing the solvent is net unfavorable, the PMF will rise. Thus, the PMF provides a clean report of the contributions of solvent to the free energy of each host-guest association.

The guest in all cases is a single, spherical "atom" of radius 5.0 Å, which interacts with both the host and the water molecules with a PHSP, which has no attractive component and has a steeply rising repulsive component that approximates a hard-sphere potential but can be accommodated in an MD simulation. This guest is large enough to displace all water molecules from the binding cavity of the host cucurbit[8]uril (CB8) (Figure 1E) but, as noted above, small enough to enter CB8 along the latter's axis of symmetry without generating steric clashes. As summarized in Figure 1, all hosts studied here share the structure of CB8. All host atoms are treated as fixed in position and interact with the guest via a PHSP. The baseline CB8 model interacts with water via a standard force field potential comprising Lennard-Jones interactions and partial charges. Additional CB8 models explore the consequences of either reduced or strengthened attractive host interactions with water.

The following subsections provide further details of these models and the computational methods.

2.2 Pseudo-Hard-Sphere Guest

2.2.1 Pseudo-Hard Potential Function

To focus on solvent contributions to binding free energy, we designed an extremely simple "guest molecule", i.e., one with a simple shape, no internal degrees of freedom, no attractive interactions with either the host or the water, and a repulsive potential that approximates a hard-wall potential, generating steric interactions while making only minimal contributions to the mean potential energy of the system. In particular, the steeper the rise of the repulsive potential with distance, the better. Accordingly, the guest is modeled as a single spherical "atom" of radius 5 Å, which is large enough to displace all water from the host cavity but small enough to pass through the carbonyl portals without generating steric clashes, and having an interaction potential that approximates the "hard wall" potential given by

$$\Phi_{\text{hard sphere}}(r_{ij}) = \begin{cases} \infty, & r_{ij} \leq \sigma \\ 0, & r_{ij} > \sigma \end{cases},$$

1

where σ determines the particle size and r_{ij} is the interatomic distance. A true hard-wall potential cannot be used in a molecular dynamics (MD) simulation as the interatomic force is undefined at $r_{ij} = \sigma$. Therefore, we sought a differentiable approximation to $\Phi_{\text{hard sphere}}$, i.e., an intermolecular potential with no attractive component and a steeply increasing repulsive component.

However, designing a sufficiently "hard" potential for a 5 Å atom was not straightforward despite the popularity of hard-sphere models. We initially tried the cut-and-shifted Weeks-Chandler-Anderson (WCA) perturbation[55] of the Lennard-Jones (LJ) potential:

$$\Phi_{\text{WCA-repulsive}}^{\text{LJ}}(r_{ij}) = \begin{cases} \Phi_{\text{LJ}}(r_{ij}) + \epsilon, & r_{ij} \leq R_{\text{min}}^{\text{LJ}} \\ 0, & r_{ij} > R_{\text{min}}^{\text{LJ}} \end{cases}.$$

2

with

$$\Phi_{\text{LJ}}(r_{ij}) = 4\epsilon \left[\left(\frac{\sigma}{r_{ij}} \right)^{12} - \left(\frac{\sigma}{r_{ij}} \right)^{6} \right],$$

3

where ϵ is the depth of the LJ energy minimum located at

$$r_{ij} = R_{\min}^{\text{LJ}} = \sigma 2^{\frac{1}{6}}. \tag{4}$$

However, simulations with this potential still yielded configurations with waters significantly closer than 5 Å from the center of the atom, leading to significantly positive mean interaction potentials. This problem results from the fact that increasing the value of σ softens the repulsive wall, as shown in the Extended Data Figure 1A. Therefore, we substituted the more general Mie potential[56] for the LJ potential:

$$\Phi_{\text{Mie}}(r_{ij}) = \frac{c_r}{c_r - c_a}\left(\frac{c_r}{c_a}\right)^{\frac{c_a}{c_r - c_a}}\epsilon\left[\left(\frac{\sigma}{r_{ij}}\right)^{c_r} - \left(\frac{\sigma}{r_{ij}}\right)^{c_a}\right], \tag{5}$$

where c_r and c_a are the exponents of the repulsive and attractive terms, respectively. The minimum of the generalized Mie potential is positioned at

$$R_{\min}^{\text{Mie}} = \sigma\left(\frac{c_r}{c_a}\right)^{\frac{1}{c_r - c_a}}, \tag{6}$$

and the WCA repulsive perturbation to the Mie potential is

$$\Phi_{\text{WCA-repulsive}}^{\text{Mie}}(r_{ij}) = \begin{cases} \Phi_{\text{Mie}}(r_{ij}) + \epsilon, & r_{ij} \leq R_{\min}^{\text{Mie}} \\ 0, & r_{ij} > R_{\min}^{\text{Mie}} \end{cases}. \tag{7}$$

Coefficients of $c_r = 50$ and $c_a = 49$ were chosen for the repulsive and attractive terms, respectively, following Jover et al.[56] However, for larger values of σ, the repulsive potential changes are, again, no longer as steep as desired (Extended Data Figure 1B). To remedy this, we introduced a distance shift using a new variable, R_{particle}, which controls the particle size instead of σ,

$$r_{ij}' = r_{ij} - \left(R_{\text{particle}} - R_{\min}^{\text{Mie}}\right), \tag{8}$$

yielding what appears to be a novel approximation to the hard-sphere potential for use in simulations:

$$\Phi_{\text{WCA-repulsive}}^{\text{Mie}}(r_{ij}') = \begin{cases} \Phi_{\text{Mie}}(r_{ij}') + \epsilon, & r_{ij} \leq R_{\text{particle}} \\ 0, & r_{ij} > R_{\text{particle}} \end{cases}. \tag{9}$$

Values of 3 Å and 0.1 kcal/mol were used for σ and ϵ, respectively, and a particle radius R_{particle} of 5 Å.

2.2.2 Hydration Free Energy of the Pseudo-Hard-Sphere Particle

We use physical (path-based) and alchemical free energy calculations to compute the hydration free energy (HFE), $\Delta G_{\text{hyd,sphere}}$, of our PHSP guest. In the alchemical calculations, we introduce a softcore potential function into Eq (5) to prevent the end-point catastrophe[57], giving us an alchemically-modified, generalized Mie potential[58]

$$\Phi_{\text{softcore}}^{\text{Mie}}(r_{ij}, \lambda) = \frac{c_r}{c_r - c_a}\left(\frac{c_r}{c_a}\right)^{\frac{c_a}{c_r - c_a}}\lambda\epsilon\left[\frac{1}{\left[\alpha(1-\lambda) + \left(\frac{r_{ij}}{\sigma}\right)^{c_a}\right]^{\frac{c_r}{c_a}}} - \frac{1}{\alpha(1-\lambda) + \left(\frac{r_{ij}}{\sigma}\right)^{c_a}}\right]. \tag{10}$$

Note that the location of the minimum varies with the coupling parameter λ:

$$R_{\min}^{\text{Mie-softcore}}(\lambda) = \sigma \left[\left(\frac{c_r}{c_a} \right)^{\frac{c_a}{c_r - c_a}} - \alpha(1-\lambda) \right]^{\frac{1}{c_a}}. \qquad \text{11}$$

Inserting the potential above in the cut-and-shifted WCA perturbation of Eq (9) gives

$$\Phi_{\text{WCA-repulsive}}^{\text{Mie-softcore}}(r_{ij}', \lambda) = \begin{cases} \Phi_{\text{Mie}}^{\text{softcore}}(r_{ij}', \lambda) + \lambda\epsilon, & r_{ij} \leq R_{\text{particle}} \\ 0, & r_{ij} > R_{\text{particle}} \end{cases}. \qquad \text{12}$$

The alchemical calculations were performed over 15 windows (λ = 0.0, 0.05, 0.1, 0.15, 0.2, 0.25, 0.3, 0.35, 0.4, 0.5, 0.6, 0.7, 0.8, 0.9, 1.0). The simulation temperature and pressure were maintained at 298.15 K and 1 bar, respectively. For each window, we ran an energy minimization, followed by 1 ns of equilibration and 10 ns of production. The free energy was estimated using the Multistate Bennett-Acceptance-Ratio (MBAR) method[59].

As a numerical check of the alchemical method, we also computed the hydration free energy using a physical path-based method. To do this, we extended the periodic box vector in the z-axis by 40 Å, creating a vacuum region in the system, and simulated the system with the NVT ensemble. Water molecules were prevented from drifting with a flat-bottomed, harmonic wall restraint with a spring constant of 10 kcal/mol/Å^2, co-centered with the water-filled region and with its two walls positioned 5 Å above the upper (z large) and below (z small) the z boundaries of the initial water-filled region. Restraints of 1 kcal/mol/Å^2 were applied to the PHSP particle at intervals along the z-axis to define 31 umbrella sampling windows over a distance of 30 Å. We ran the same amount of sampling as in our alchemical calculations above, and the PMF was extracted with WHAM. The uncertainty in the PMF was estimated with 2000 steps of bootstrapping. The value of $\Delta G_{\text{hyd,sphere}}$ quantity was obtained as the difference between the PMF at z_i = 0 Å and 30 Å.

The physical and alchemical methods gave essentially the same value of $\Delta G_{\text{hyd,sphere}}$ as we varied the particle radius from 1 Å to 5 Å (Extended Data Figure S2 and Extended Data Table S1). The value of $\Delta G_{\text{hyd,sphere}}$ is positive for all radii, indicating a free energy cost of creating a spherical cavity, or bubble, in bulk water. The free energy cost increases sharply as the particle becomes larger, reaching a value of 21 kcal/mol at 5 Å, the size used in the subsequent binding (PMF) calculations. The present results, obtained with the TIP3P water model, are similar to those reported previously[60] for hydration of hard spheres of various radii with the TIP4P[61] water model. Because the PHSP potential has no attractive component and a steep-walled ("hard") repulsive component, the mean interaction potential energy of the hydrated 5 Å particle with water is only 0.30 kcal/mol – a very small value relative to the hydration free energy of 21 kcal/mol, as intended (Section 2.2). The near absence of solute-solvent interactions implies that the strongly positive hydration free energy results almost entirely from the reorganization of the water in response to the insertion of the particle (cavitation energy). These results provide a methodological foundation for the present study.

2.3 Models of the CB8 Host Molecule

All of the model hosts considered here (Figure 1) interact with the PHSP guest via Eqs (5)-(9), but we varied the character of the hosts' interactions with water. Our baseline CB8 model is assigned conventional force field nonbonded parameters (Section 2.5). To create a series of nonpolar CB8 models whose attractive LJ (dispersion) interactions with water range down to zero, we set all partial charges to zero and used the following equation to scale from full LJ interactions (NP) to the cut-and-shifted WCA potential (Hard):

$$\Phi_{\text{WCA-dispersive}}^{\text{LJ}}(r_{ij}, \lambda) = \begin{cases} \Phi_{\text{LJ}}(r_{ij}) + \epsilon(1 - \lambda), & r_{ij} \leq R_{\min}^{\text{LJ}} \\ \lambda \Phi_{\text{LJ}}(r_{ij}), & r_{ij} > R_{\min}^{\text{LJ}} \end{cases}. \qquad 13$$

Here λ is a coupling parameter between 0 and 1 that determines the strength of the LJ dispersive interactions. Using this potential provides a non-attractive host (Hard) at $\lambda = 0$ and an attractive but nonpolar host (NP) at $\lambda = 1$. The mean potential energy of interaction of the Hard host with all water in the simulation system is small and unfavorable, at 2.8 kcal/mol, consistent with the design of the pseudo-hard potential.

We also investigated CB8 models having strongly favorable electrostatic interactions with water molecules by creating capacitor-like constructs. Starting with the non-polar NP model, charges of $\pm 1e$ were placed on one (Charge1) or two (Charge2) pairs of carbon atoms symmetrically, on opposite sides of the molecule (Figure 1C). We use CB8 as the base structure, as the even-membered macrocycle CB8 – unlike CB7 - allows for the symmetric placement of opposite charges across from each other.

To compute the mean number of waters in the host cavities, we defined the cavity as a cylinder centered at the center of mass of the CB8 molecule and oriented along its axis of symmetry (z-axis, Figure 1A), with radius 6.0 Å and end-to-end length of 6.4 Å.

2.4 Potential of Mean Force Calculations

We used umbrella sampling (US) calculations with the weighted histogram analysis method (WHAM)[62] to compute potentials of mean force (PMF) for insertion of the PHSP guest into the host models along the axis of symmetry (z-axis) of the symmetric CB8 molecule (Extended Data Figure S3). The reaction coordinate is the distance, projected onto the z-axis, between the center of the monatomic guest and the center of mass (COM) of CB8. We first pull the particle out of the CB8 host with steered MD (SMD) simulation, using a spring constant of 25 kcal/mol/Å^2, from 0 Å to 15 Å. A harmonic potential with a spring constant of 100 kcal/mol/Å^2 in the *x-y* plane was used to keep the particle close to the z-axis. The velocity was set to 2 Å/ns, and snapshots from these SMD simulations were used as the starting configuration for the subsequent US calculations. To improve the overlap between neighboring umbrella windows, we stratified the umbrella windows from 0 to 5 Å with increments of 0.25 Å and a spring constant of 25 kcal/mol/Å^2 and increments of 0.5 from 5 to 15 Å with a spring constant of 10 kcal/mol/Å^2. The same harmonic potential in the x-y plane was applied for each window as in the SMD calculations to limit the particle's motion away from the z-axis. The CB8 structure is kept rigid for all calculations to remove all internal, translational, and rotational degrees of freedom.

2.5 Force Field and Simulation Details

For all CB8 model hosts, we used General Amber Force Field version 2.1 (GAFF2) LJ parameters. Note that the valence parameters are irrelevant because the molecules are treated as rigid. AM1-BCC[63,64] partial charges were generated with the *antechamber* program from AmberTools[65]. For the PMF calculations, we solvated the CB8 structure with 2500 TIP3P[61] water molecules positioned in the center of a rectangular periodic box with the *tleap* program of AmberTools. For HFE calculations, we solvated the PHSP particle or CB8 with 2000 TIP3P water molecules in a cubic box. All MD simulations were carried out with the OpenMM[66] MD engine, version 7.5.1. The short-range, direct, nonbonded interactions were truncated with a cutoff of 9 Å, and the long-range interactions were handled with the particle-mesh Ewald (PME) method[67,68]. The simulations were run in the NPT ensemble, maintaining the temperature at 298.15 K with the Langevin thermostat[69] with an integration time step of 2 fs. The system was maintained at 1.0 atmosphere pressure with the Monte Carlo barostat[70,71]. We implemented the potential functions of Eqs (5)-(13) and (10)-(12) in OpenMM[66] using the *CustomNonbondedForce* class. All the Python code used to

model the CB8 and PHSP systems and analysis used in this work is freely available on GitHub (https://github.com/jeff231li/pseudo-hard-sphere-solvation-scripts).

3 Results

3.1 The free energy of displacing water from CB8 is positive

We employed a thermodynamic cycle (Figure 2.) to determine the free energy change of fully displacing water from the binding site of the aqueous CB8 host, i.e., of forming a "bubble" in the binding site, where the bubble is created with our pseudo-hard-sphere potential (PHSP) guest (Section 2.2.1). This quantity, $\Delta G_{\mathrm{displace}}$, is given by the free energy change of moving the spherical guest, or bubble, from vacuum to water (i.e., of hydrating the guest) plus the free energy change of moving the guest into the binding site, i.e.: $\Delta G_{\mathrm{displace}} = \Delta G_{\mathrm{hyd,sphere}} + \Delta G_{\mathrm{bind}}$, where ΔG_{bind} is the change in the free energy when the sphere is moved from a fixed location in bulk water to the center of the CB8 binding cavity.
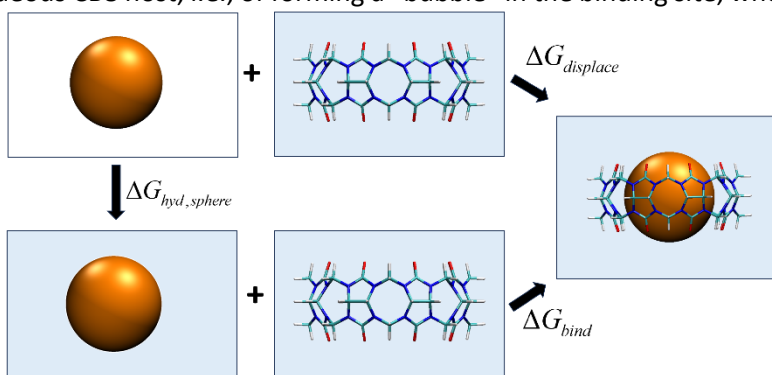

Figure 2. Thermodynamic cycle used to compute water displacement free energy. Lower process depicts binding of PHSP guest initially in water (orange sphere, lower left) with initially water-filled CB8 to form bound complex (right). Top process shows binding of PHSP guest initially in vacuum with the initially water-filled host. Left process depicts transfer of the PHSP guest from vacuum to water.

As shown in Figure 3A,D, the change in free energy upon moving the sphere from bulk water into the CB8 binding site is ΔG_{bind} = −5 kcal/mol. With $\Delta G_{\mathrm{hyd,sphere}}$ = 21 kcal/mol for this guest molecule (Section 2.2.2), we find a large free energy cost of +16 kcal/mol for displacing the binding site water. This result is consistent with the fact that the binding site is initially stably filled with 10.7 water molecules, on average (Figure 3D), while this number falls to zero when the guest is bound.

3.2 Changing the free energy of water displacement changes the binding free energy

We used the same method to determine the free energy of displacing water from the nonpolar (NP) version of the CB8 host, where all atomic partial charges have been set to zero, and from the highly polar Charge1 and Charge2 versions of CB8, where all partial charges were zeroed and then either one pair (Charge1) or two pairs (Charge2) of atoms were assigned ±1e charges to create zwitterionic hosts molecules (Figure 1).

The binding free energy of the PHSP guest with NP is considerably more favorable than for regular CB8, at ΔG_{bind} = −10.5 kcal/mol instead of −5.0 kcal/mol (Figure 3). Using our thermodynamic cycle (Figure 2), the free energy cost of displacing the 9.9 water molecules present in NP (Figure 3) is +10.5 kcal/mol (Figure 3), much lower than the water displacement cost of +16.0 kcal/mol obtained for CB8 (Section 3.1). We conclude that the water in the nonpolar NP host is less thermodynamically favorable than the water in CB8 with its full complement of partial charges. This makes sense because, unlike native CB8, the fully nonpolar NP host cannot make favorable electrostatic interactions with the cavity water.

In contrast, the binding free energies of the PHSP guest with the highly polar Charge1 and Charge2 models of the CB8 macrocycle are unfavorable, at +3.0 kcal/mol and +15.7 kcal/mol, respectively (Figure 3). This is because, as determined from the same thermodynamic cycle, the costs of water displacement have increased sharply to 24.0 kcal/mol and 36.7 kcal/mol, respectively (Figure 3). However, the mean number of waters initially in the binding site is essentially unchanged, at 10.5 and 11.0, respectively (Figure 3). We conclude that the water in these highly polar hosts is much more thermodynamically favorable than the water in native CB8, due to the strong electrostatic interactions between the cavity water and the ionic charges of the hosts.

CB8 Model	N_{water}	$\Delta G_{displace}$	ΔG_{bind}
Hard (λ=0)	0.0	0.3	−20.7
λ=0.5	1.4	0.9	−20.1
λ=0.6	4.8	1.9	−19.1
λ=0.7	7.0	4.0	−17.0
λ=0.8	7.9	5.7	−15.3
λ=0.9	8.4	8.1	−12.9
NP (λ=1)	9.9	10.5	−10.5
CB8	**10.7**	**16.0**	**−5.0**
Charge1	10.5	24.0	3.0
Charge2	11.0	36.7	15.7
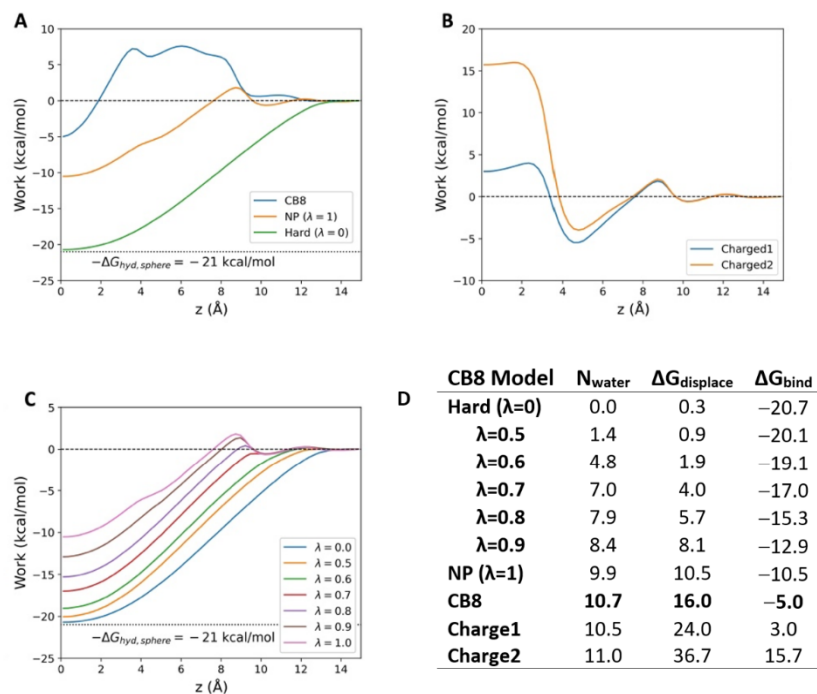
Figure 3. Computed thermodynamics of host-guest binding for model systems. A) Potentials of mean force (PMF) of pushing water molecules out of the CB8 cavity using the PHSP particle for CB8 (standard force field), NP, and Hard host models. B) PMFs for the charged models Charge1 and Charge2, C) PMFs for Hard model CB8 with intermediate strength dispersion interactions (λ=0 to 1). D) Table showing, for each host considered in A-C, the mean number of waters in the binding cavity, the binding free energy (kcal/mol), and the water displacement free energy (kcal/mol). The number of water molecules in the cavity is estimated for a cylindrical region centered on the host with radius 6.0 Å and height of ±3.2 Å from the center of mass of CB8.

3.3 Dewetting can further affect the free energies of water displacement and binding

Increasingly dewetted binding cavities, with mean water occupancies approaching zero, can be obtained by not only setting the partial charges of a model CB8 host to zero but also scaling its Lennard-Jones interactions with water from full LJ interactions (λ = 1, corresponding to host NP) down to a pseudo-hard potential with no attractive component for λ = 0 (corresponding to host Hard). The mean number of waters in the cavity decreases steadily with decreasing lambda, with λ = 0 leading to essentially complete drying (Figure 3). Concurrently, the binding free energy becomes increasingly favorable, reaching −21 kcal/mol for the fully dewetted λ = 0 case (Figure 3A,D). At the same time, the free energy cost of displacing water molecules drops to zero (Figure 3), consistent with the absence of water molecules to displace from the fully dewetted cavity—or nearly so, given that the occupancy of spatially accessible cavities cannot fall below the residual threshold expected for water in the gas phase.

4 Discussion

The free energy cost of displacing water from a binding cavity is greater than or equal to zero across all model hosts studied here. In this sense, water is stably present in the binding cavities of these hosts. However, the degree of stability varies, with the cost of water displacement ranging from 0 for the fully dewetted Hard host to +37 kcal/mol for the strongly polar Charge2 host. Because the free energy of dehydrating the spherical guest is the same across all of the macrocyclic hosts, and the interaction energy of all hosts with the guest is near zero, due to the pseudo-hard-sphere character of the guest, the initial thermodynamic state of the cavity water is the key determinant of affinity across this series of chemically different macrocycles. Accordingly, the free energies of binding range from −21 kcal/mol for the Hard host, where there is no water to be displaced, to +16 kcal/mol for Charge2, where the binding site water is tightly bound to the ionic host.

These results support the concept that a host molecule's ability to achieve high affinity depends on the presence of "unfavorable" binding site water. Cucurbiturils, for example, are known for their high binding affinities, attributed to their binding sites containing particularly unfavorable water. This is due to their barrel shape and nonpolar interiors[72], which deprive water molecules of the favorable interactions they typically have in bulk. In contrast, water in the binding sites of more open, polar, or aromatic hosts—such as cyclodextrins, calixarenes, cyclophanes, and hemicarcerands—is expected to be more thermodynamically favored, making its displacement less contributory to binding[14]. It should be noted that the present calculations artificially isolate changes in water thermodynamics as the primary driver of binding, since the spherical guest is designed to have essentially zero direct interaction with the hosts. Experimentally, attractive forces between the guest and the host also contribute to binding and must be optimized to maximize affinity. However, in view of the present results, it is possible to achieve high binding affinities even without *any* optimization of attractive forces between host and guest.

It may seem paradoxical that thermodynamically unfavorable water can be stably present in a binding site, such as in the NP host. Indeed, one could argue that, if the water inside a cavity is of "high free energy", it has no reason to remain there. However, spontaneous dewetting of our model CB8 binding sites is not thermodynamically favored until virtually all attractive interactions with water are artificially eliminated, as in the Hard host.
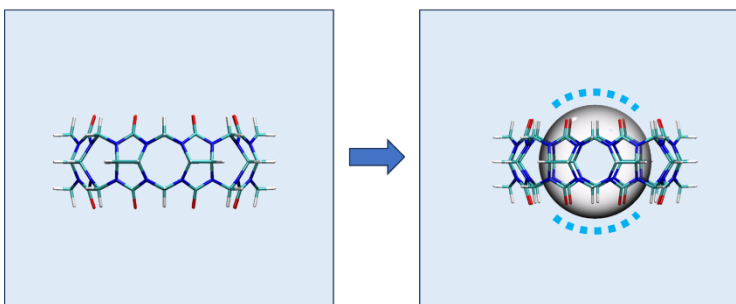

Figure 4. Hypothetical spontaneous dewetting of CB8 host generates a bubble within the binding cavity. The dashed blue lines indicate thermodynamically unfavorable water at the surface of the bubble.

This may seem surprising, as the transfer of water from the cavity to the bulk would allow the thermodynamically unfavorable cavity water to adopt the more energetically favorable properties of bulk water. The explanation for how thermodynamically unfavorable water can still be stably present in the binding cavity is that complete dewetting would create a new vapor-liquid interface at the boundary of the dewetted region (Figure 4), and the liquid water at this interface (dashed lines in Figure 4) would itself be thermodynamically unfavorable, and the net effect would be to raise the overall free energy of the host-water system. More generally, it is essential, when analyzing the thermodynamics of dewetting, is crucial to consider both the initial and proposed final states.

Given that the native CB8 cavity is stably solvated, it may be tempting to conclude that its thermodynamically favorable binding reaction is driven instead by the desolvation of the nonpolar guest. However, spontaneous dewetting of the guest is also thermodynamically disfavored, or else it would be surrounded by a vapor bubble. Thus, we have a situation in which binding could appear to be driven by two dehydration processes that are both unfavorable: that of the guest and that of the cavity of the host. Correct conclusions are reached if we take a holistic view of the contribution of water to binding by considering the amount of unfavorable vs. favorable water present in the initial vs. final states of the system,
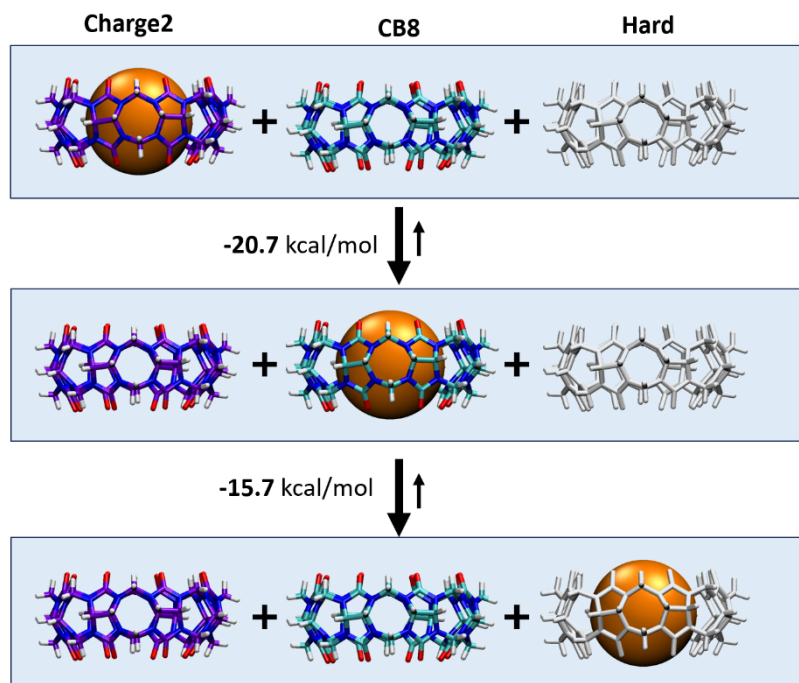

Figure 5. "Isodesmic" reactions highlight the contribution of water thermodynamics to binding. The hard-sphere guest (orange) binds most weakly to the Charge2 model, where cavity water is most stable, and most strongly to the Hard host model, where cavity water is least stable. The free energies are based on the results from Figure 3.

without considering hypothetical dewetted or dehydrated states that do not arise in the actual system. The theory of the free energy density of fluids provides a rigorous foundation for this form of analysis[12]. Another informative way to focus on the role of water in binding is illustrated in Figure 5, where two "isodesmic" reactions are driven by the fact that water strongly prefers to be within the Charge2 binding site over being within the binding site of native CB8, and that there is no free energy penalty for displacement of water from the Hard host on binding as it is already dewetted. Accordingly, if these reactions were to occur in vacuum, rather than in water, their free energy changes would be zero.

It has been suggested that "water's influence on the free energy driving force for any aqueous self-assembly necessarily depends entirely on the direct interactions between the solute species with each other and with water, rather than on indirect solute-induced changes in water-water interaction energy and entropy,"[49], and a similar view has been expressed elsewhere[73]. However, we observe strong binding of the PHSP guest with the Hard model host (ΔG_{bind} = −21 kcal/mol), even though the energetic host-guest, host-water, and guest-water interactions are weak and purely repulsive, and the changes in internal energy and configurational entropy of the host and guest are zero, since these idealized solutes have no internal degrees of freedom. Therefore, the strongly favorable binding free energy results purely from changes of water upon binding. Intuitively, binding is thermodynamically favored because it allows the free energy of the solvent – the volume integral of its free energy density[12] – to fall.

Although the free energy costs of displacing water from the NP (λ = 1), CB8, Charge1, and Charge2 hosts range over 28 kcal/mol, the mean number of cavity waters they contain is essentially constant, at 10.5±0.6 (Figure 3D and Figure 6), which fully aligns with the expected number of water molecules inside the CB8

cavity[10,11,27,28]. The insensitivity of N_{water} to the strength of the attractive forces in this regime results from liquid water's low compressibility. In contrast, the more artificial host constructs with partial charges set to zero and $\lambda < 1$ show progressive dewetting as λ falls until finally $N_{\text{water}} = 0$ for $\lambda = 0$ (Hard model). Consistent with the weakening attractive forces between the host and the water and the falling number of waters to be displaced, the work of water displacement also falls, reaching a limiting value of 0 for the Hard model. However, these displacement free energies span only about 10 kcal/mol. Thus, although this dewetting is an interesting phenomenon, we observe a larger thermodynamic variation among the host models that are fully hydrated (with liquid water). This demonstrates that, in the most common and experimentally most relevant setting of well-hydrated binding cavities, water displaceability can vary widely without dewetting and correlates poorly, if at all, with water density. Although dewetting may occur in small, highly nonpolar cavities and tubes[14,52], dewetting of binding sites is the exception to the rule that there is no vacuum in water, and most attention should be given to the more practically relevant situation of fully solvated hosts and guests.

As a key result, we observe a biphasic relationship between water density and the free energy of displacement (Figure 6). Thus, progressively eliminating all attractive host-water interactions leads to progressive dewetting, i.e. drying, of the cavity (lower left of graph) but only modest changes in the free energy of water displacement, whereas progressively strengthening of attractive host-water interactions causes no significant change in water density but dramatically increases the free energy cost of water displacement (far right of graph).

The excess chemical potential of water at a given location, $\mu_{ex}(R)$, is the free energy of inserting a water molecule at R^{74} so it might be expected to correlate with the thermodynamic favorability of water in our model host cavities. Because $\mu_{ex}(R)$ varies linearly with $\ln \rho(R)^{74,75}$, where $\rho(R)$ is the number density of water, and because all of the present model hosts have cavities of identical volume, we can test this expectation by looking for a linear relationship between $\Delta G_{\text{displace}}$ and $\ln N_{\text{water}}$. From Figure 6 and Extended Data Figure S4, however, it is clear that this relationship does not hold, particularly among the more realistic water-filled CB8 models on the right-hand side of the graph. Thus, neither the density nor the excess chemical potential of water is a reliable indicator of the thermodynamic favorability of liquid water.
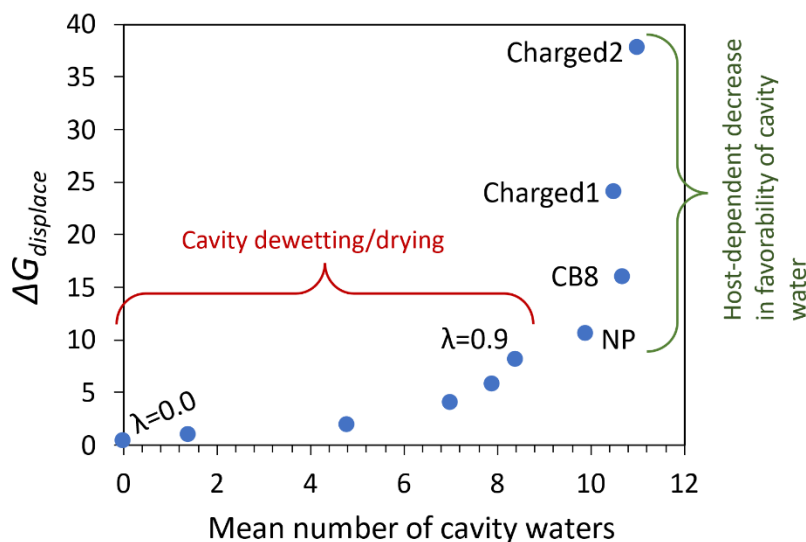

Figure 6. Relationship between the free energy of water displacement, $\Delta G_{\text{displace}}$ (kcal/mol) and the mean number of cavity waters, for each model host-guest system. Data are drawn from Figure 2D. Curly brackets highlight the biphasic character of the plotted relationship.

As to the chemical potential of water, this quantity is fundamentally not a position-dependent quantity. Rather, it is the change in free energy of adding one water molecule to the system, so it is influenced by all positions in the system that a water molecule accesses.

5   Conclusions

The present computational analysis of simplified host-guest systems clearly shows that binding affinities are strongly influenced by the thermodynamic properties of the water displaced from binding sites. These thermodynamic properties of water, and the associated favorability of water displacement, vary strongly with the chemical nature of the host. The results also demonstrate that significant cavity dewetting or drying can be observed as a special, extreme case, for example when polar interactions are removed and dispersion interactions are artificially reduced, and this effect can further promote host-guest binding. Interestingly, neither water density nor excess chemical potential reliably indicates the thermodynamic favorability of cavity water. Although our hosts all share the structural framework of a cucurbituril, the concepts developed here are applicable to other macromolecular host molecules and, thus, can be broadly useful to explain observations and guide the design of drugs and supramolecular systems.

6   Acknowledgements

7   Author Disclosures

MKG has an equity interest in and is a cofounder and scientific advisor of VeraChem LLC. He is also a scientific advisor to Denovicon Therapeutics, Beren Therapeutics, and In Cerebro Inc.

8   References

(1) VanEtten, R. L.; Sebastian, J. F.; Clowes, G. A.; Bender, M. L. Acceleration of Phenyl Ester Cleavage by Cycloamyloses. A Model for Enzymic Specificity. *J. Am. Chem. Soc.* **1967**, *89* (13), 3242–3253. https://doi.org/10.1021/ja00989a027.

(2) Griffiths, D. W.; Bender, M. L. Cycloamyloses as Catalysts. In *Advances in Catalysis*; Eley, D. D., Pines, H., Weisz, P. B., Eds.; Academic Press, 1973; Vol. 23, pp 209–261. https://doi.org/10.1016/S0360-0564(08)60302-8.

(3) Connors, K. A. The Stability of Cyclodextrin Complexes in Solution. *Chem Rev* **1997**, *97*, 13251357.

(4) Kauzmann, W. Some Factors in the Interpretation of Protein Denaturation. *Adv Prot Chem* **1959**, *14*, 1–63.

(5) Smithrud, D. B.; Wyman, T. B.; Diederich, F. Enthalpically Driven Cyclophane-Arene Inclusion Complexation: Solvent-Dependent Calorimetric Studies. *J. Am. Chem. Soc.* **1991**, *113* (14), 5420–5426. https://doi.org/10.1021/ja00014a038.

(6) Kubik, S. When Molecules Meet in Water-Recent Contributions of Supramolecular Chemistry to the Understanding of Molecular Recognition Processes in Water. *ChemistryOpen* **2022**, *11* (4), e202200028. https://doi.org/10.1002/open.202200028.

(7) Young, T.; Abel, R.; Kim, B.; Berne, B. J.; Friesner, R. A. Motifs for Molecular Recognition Exploiting Hydrophobic Enclosure in Protein-Ligand Binding. *Proc. Natl. Acad. Sci. U. S. A.* **2007**, *104* (3), 808–813. https://doi.org/10.1073/pnas.0610202104.

(8) Snyder, P. W.; Lockett, M. R.; Moustakas, D. T.; Whitesides, G. M. Is It the Shape of the Cavity, or the Shape of the Water in the Cavity? *Eur. Phys. J. Spec. Top.* **2014**, *223* (5), 853–891. https://doi.org/10.1140/epjst/e2013-01818-y.

(9) Saenger, W.; Noltemeyer, M.; Manor, P. C.; Hingerty, B.; Klar, B. "Induced-Fit"-Type Complex Formation of the Model Enzyme α-Cyclodextrin. *Bioorganic Chem.* **1976**, *5* (2), 187–195. https://doi.org/10.1016/0045-2068(76)90007-9.

(10) Chacko, K. K.; Saenger, W. Topography of Cyclodextrin Inclusion Complexes. 15. Crystal and Molecular Structure of the Cyclohexaamylose-7.57 Water Complex, Form III. Four- and Six-Membered Circular Hydrogen Bonds. *J. Am. Chem. Soc.* **1981**, *103* (7), 1708–1715. https://doi.org/10.1021/ja00397a021.

(11) Haider, K.; Wickstrom, L.; Ramsey, S.; Gilson, M. K. Enthalpic Breakdown of Water Structure on Protein Active-Site Surfaces. *J. Phys. Chem. B* **2016**.

(12) Gilson, M. K.; Kurtzman, T. Free Energy Density of a Fluid and Its Role in Solvation and Binding. *J. Chem. Theory Comput.* **2024**, *20* (7), 2871–2887. https://doi.org/10.1021/acs.jctc.3c01173.

(13) Ewell, J.; Gibb, B. C.; Rick, S. W. Water inside a Hydrophobic Cavitand Molecule. *J. Phys. Chem. B* **2008**, *112* (33), 10272–10279. https://doi.org/10.1021/jp804429n.

(14) Biedermann, F.; Nau, W. M.; Schneider, H.-J. The Hydrophobic Effect Revisited—Studies with Supramolecular Complexes Imply High-Energy Water as a Noncovalent Driving Force. *Angew. Chem. Int. Ed.* **2014**, *53* (42), 11158–11171. https://doi.org/10.1002/anie.201310958.

(15) Usenik, A.; Leko, K.; Petrović Peroković, V.; Car, Ž.; Ribić, R.; Pičuljan, K.; Hanževački, M.; Draženović, J.; Požar, J. Hydrophobically Driven Hosting – What about the Guest? *J. Mol. Liq.* **2023**, *388*, 122774. https://doi.org/10.1016/j.molliq.2023.122774.

(16) Metherell, A. J.; Cullen, W.; Williams, N. H.; Ward, M. D. Binding of Hydrophobic Guests in a Coordination Cage Cavity Is Driven by Liberation of "High-Energy" Water. *Chem. – Eur. J.* **2018**, *24* (7), 1554–1560. https://doi.org/10.1002/chem.201704163.

(17) Kanagaraj, K.; Alagesan, M.; Inoue, Y.; Yang, C. Solvation Effects in Supramolecular Chemistry. In *Comprehensive Supramolecular Chemistry II*; Atwood, J. L., Ed.; Elsevier: Oxford, 2017; pp 11–60. https://doi.org/10.1016/B978-0-12-409547-2.12481-3.

(18) Venkataramanan, N. S.; Suvitha, A.; Sahara, R. Structure, Stability, and Nature of Bonding between High Energy Water Clusters Confined inside Cucurbituril: A Computational Study. *Comput. Theor. Chem.* **2019**, *1148*, 44–54. https://doi.org/10.1016/j.comptc.2018.12.015.

(19) Escobar, L.; Ballester, P. Molecular Recognition in Water Using Macrocyclic Synthetic Receptors. *Chem. Rev.* **2021**, *121* (4), 2445–2514. https://doi.org/10.1021/acs.chemrev.0c00522.

(20) Poulson, B. G.; Alsulami, Q. A.; Sharfalddin, A.; El Agammy, E. F.; Mouffouk, F.; Emwas, A.-H.; Jaremko, L.; Jaremko, M. Cyclodextrins: Structural, Chemical, and Physical Properties, and Applications. *Polysaccharides* **2022**, *3* (1), 1–31. https://doi.org/10.3390/polysaccharides3010001.

(21) Alešković, M.; Šekutor, M. Overcoming Barriers with Non-Covalent Interactions: Supramolecular Recognition of Adamantyl Cucurbit[n]Uril Assemblies for Medical Applications. *RSC Med. Chem.* **2024**, *15* (2), 433–471. https://doi.org/10.1039/D3MD00596H.

(22) Liu, S.; Rupic, C.; Mukhpadhayay, P.; Chakrabarti, S.; Zavalij, P. Y.; Isaacs, L. The Cucurbit[n]Uril Family: Prime Components for Self-Sorting Systems. *J Am Chem Soc* **2005**, *127*, 15959–15967.

(23) Cao, L.; Šekutor, M.; Zavalij, P.; Mlinarić-Majerski, K.; Glaser, R.; Isaacs, L. D. Cucurbit[7]Uril·guest Pair with an Attomolar Dissociation Constant. *Angew. Chem. Int. Ed.* **2014**, *53* (4), 988–993. https://doi.org/10.1002/ANIE.201309635.

(24) Kim, K.; Selvapalam, N.; Oh, D. H. Cucurbiturils–a New Family of Host Molecules. *J. Incl. Phenom. Macrocycl. Chem.* **2004**, *50* (1), 31–36. https://doi.org/10.1007/s10847-004-8835-7.

(25) Rekharsky, M. V.; Mori, T.; Yang, C.; Ko, Y. H.; Selvapalam, N.; Kim, H.; Sobransingh, D.; Kaifer, A. E.; Liu, S.; Isaacs, L.; Chen, W.; Moghaddam, S.; Gilson, M. K.; Kim, K.; Inoue, Y. A Synthetic Host-Guest System Achieves Avidin-Biotin Affinity by Overcoming Enthalpy–Entropy Compensation. *Proc Nat Acad Sci USA* **2007**, *104* (52), 20737–20742. https://doi.org/10.1073/pnas.0706407105.

(26) Marquez, C.; Hudgins, R. R.; Nau, W. M. Mechanism of Host-Guest Complexation by Cucurbituril. *J Am Chem Soc* **2004**, *126*, 5806–5816.

(27) Nau, W. M.; Florea, M.; Assaf, K. I. Deep Inside Cucurbiturils: Physical Properties and Volumes of Their Inner Cavity Determine the Hydrophobic Driving Force for Host–Guest Complexation. *Isr. J. Chem.* **2011**, *51* (5–6), 559–577. https://doi.org/10.1002/ijch.201100044.

(28) Nguyen, C. N.; Kurtzman Young, T.; Gilson, M. K. Grid Inhomogeneous Solvation Theory: Hydration Structure and Thermodynamics of the Miniature Receptor Cucurbit[7]Uril. *J. Chem. Phys.* **2012**, *137* (4), 044101. https://doi.org/doi:10.1063/1.4733951.

(29) Biedermann, F.; Uzunova, V. D.; Scherman, O. A.; Nau, W. M.; De Simone, A. Release of High-Energy Water as an Essential Driving Force for the High-Affinity Binding of Cucurbit[n]Urils. *J. Am. Chem. Soc.* **2012**, *134* (37), 15318–15323. https://doi.org/10.1021/ja303309e.

(30) Biedermann, F.; Vendruscolo, M.; Scherman, O. A.; De Simone, A.; Nau, W. M. Cucurbit[8]Uril and Blue-Box: High-Energy Water Release Overwhelms Electrostatic Interactions. *J. Am. Chem. Soc.* **2013**, *135* (39), 14879–14888. https://doi.org/10.1021/ja407951x.

(31) Beuming, T.; Farid, R.; Sherman, W. High-Energy Water Sites Determine Peptide Binding Affinity and Specificity of PDZ Domains. *Protein Sci. Publ. Protein Soc.* **2009**, *18* (8), 1609–1619. https://doi.org/10.1002/pro.177.

(32) Wang, L.; Berne, B. J.; Friesner, R. A. Ligand Binding to Protein-Binding Pockets with Wet and Dry Regions. *Proc. Natl. Acad. Sci.* **2011**, *108* (4), 1326–1330. https://doi.org/10.1073/pnas.1016793108.

(33) Haider, K.; Cruz, A.; Ramsey, S.; Gilson, M. K.; Kurtzman, T. Solvation Structure and Thermodynamic Mapping (SSTMap): An Open-Source, Flexible Package for the Analysis of Water in Molecular Dynamics Trajectories. *J. Chem. Theory Comput.* **2018**, *14* (1), 418–425.

(34) Cappel, D.; Sherman, W.; Beuming, T. Calculating Water Thermodynamics in the Binding Site of Proteins – Applications of WaterMap to Drug Discovery. *Curr. Top. Med. Chem.* **2017**, *17* (23), 2586–2598. https://doi.org/10.2174/1568026617666170414141452.

(35) Abel, R.; Wang, L.; Friesner, R. A.; Berne, B. J. A Displaced-Solvent Functional Analysis of Model Hydrophobic Enclosures. *J. Chem. Theory Comput.* **2010**, *6* (9), 2924–2934. https://doi.org/10.1021/ct100215c.

(36) Cui, D.; Zhang, B. W.; Matubayasi, N.; Levy, R. M. The Role of Interfacial Water in Protein–Ligand Binding: Insights from the Indirect Solvent Mediated Potential of Mean Force. *J. Chem. Theory Comput.* **2018**, *14* (2), 512–526. https://doi.org/10.1021/acs.jctc.7b01076.

(37) Kamps, J. J. A. G.; Huang, J.; Poater, J.; Xu, C.; Pieters, B. J. G. E.; Dong, A.; Min, J.; Sherman, W.; Beuming, T.; Matthias Bickelhaupt, F.; Li, H.; Mecinović, J. Chemical Basis for the Recognition of Trimethyllysine by Epigenetic Reader Proteins. *Nat. Commun.* **2015**, *6* (1), 8911. https://doi.org/10.1038/ncomms9911.

(38) Nguyen, C. N.; Cruz, A.; Gilson, M. K.; Kurtzman, T. Thermodynamics of Water in an Enzyme Active Site: Grid-Based Hydration Analysis of Coagulation Factor Xa. *J. Chem. Theory Comput.* **2014**, *10* (7), 2769–2780. https://doi.org/10.1021/ct401110x.

(39) Lazaridis, T. Inhomogeneous Fluid Approach to Solvation Thermodynamics. 1. Theory. *J. Phys. Chem. B* **1998**, *102* (18), 3531–3541. https://doi.org/10.1021/jp9723574.

(40) Wickstrom, L.; Deng, N.; He, P.; Mentes, A.; Nguyen, C.; Gilson, M. K.; Kurtzman, T.; Gallicchio, E.; Levy, R. M. Parameterization of an Effective Potential for Protein--Ligand Binding from Host--Guest Affinity Data. *J. Mol. Recognit.* **2016**, *29* (1), 10–21.

(41) Schauperl, M.; Podewitz, M.; Waldner, B. J.; Liedl, K. R. Enthalpic and Entropic Contributions to Hydrophobicity. *J. Chem. Theory Comput.* **2016**, *12* (9), 4600–4610. https://doi.org/10.1021/acs.jctc.6b00422.

(42) Gallicchio, E.; Kubo, M. M.; Levy, R. M. Enthalpy–Entropy and Cavity Decomposition of Alkane Hydration Free Energies: Numerical Results and Implications for Theories of Hydrophobic Solvation. *J. Phys. Chem. B* **2000**, *104* (26), 6271–6285. https://doi.org/10.1021/jp0006274.

(43) Olson, B.; Cruz, A.; Chen, L.; Ghattas, M.; Ji, Y.; Huang, K.; Ayoub, S.; Luchko, T.; McKay, D. J.; Kurtzman, T. An Online Repository of Solvation Thermodynamic and Structural Maps of SARS-CoV-2 Targets. *J. Comput. Aided Mol. Des.* **2020**, *34* (12), 1219–1228. https://doi.org/10.1007/s10822-020-00341-x.

(44) Berne, B. J.; Weeks, J. D.; Zhou, R. Dewetting and Hydrophobic Interaction in Physical and Biological Systems. *Annu. Rev. Phys. Chem.* **2009**, *60*, 85–103. https://doi.org/10.1146/annurev.physchem.58.032806.104445.

(45) Aldeghi, M.; Ross, G. A.; Bodkin, M. J.; Essex, J. W.; Knapp, S.; Biggin, P. C. Large-Scale Analysis of Water Stability in Bromodomain Binding Pockets with Grand Canonical Monte Carlo. *Commun. Chem.* **2018**, *1* (1), 1–12. https://doi.org/10.1038/s42004-018-0019-x.

(46) Chiara Storer, M.; A. Hunter, C. The Surface Site Interaction Point Approach to Non-Covalent Interactions. *Chem. Soc. Rev.* **2022**, *51* (24), 10064–10082. https://doi.org/10.1039/D2CS00701K.

(47) Cremer, P. S.; Flood, A. H.; Gibb, B. C.; Mobley, D. L. Collaborative Routes to Clarifying the Murky Waters of Aqueous Supramolecular Chemistry. *Nat. Chem.* **2018**, *10* (1), 8. https://doi.org/10.1038/nchem.2894.

(48) de Oliveira, D. M.; Ben-Amotz, D. Cavity Hydration and Competitive Binding in Methylated β-Cyclodextrin. *J. Phys. Chem. Lett.* **2019**, *10* (11), 2802–2805. https://doi.org/10.1021/acs.jpclett.9b00939.

(49) Ben-Amotz, D. Hydration-Shell Vibrational Spectroscopy. *J. Am. Chem. Soc.* **2019**, *141* (27), 10569–10580. https://doi.org/10.1021/jacs.9b02742.

(50) Ashbaugh, H. S.; Gibb, B. C.; Suating, P. Cavitand Complexes in Aqueous Solution: Collaborative Experimental and Computational Studies of the Wetting, Assembly, and Function of Nanoscopic Bowls in Water. *J. Phys. Chem. B* **2021**, *125* (13), 3253–3268. https://doi.org/10.1021/acs.jpcb.0c11017.

(51) Suating, P.; Ernst, N. E.; Alagbe, B. D.; Skinner, H. A.; Mague, J. T.; Ashbaugh, H. S.; Gibb, B. C. On the Nature of Guest Complexation in Water: Triggered Wetting–Water-Mediated Binding. *J. Phys. Chem. B* **2022**, *126* (16), 3150–3160. https://doi.org/10.1021/acs.jpcb.2c00628.

(52) He, S.; Biedermann, F.; Vankova, N.; Zhechkov, L.; Heine, T.; Hoffman, R. E.; De Simone, A.; Duignan, T. T.; Nau, W. M. Cavitation Energies Can Outperform Dispersion Interactions. *Nat. Chem.* **2018**, *10*, 1252–1257. https://doi.org/10.1038/s41557-018-0146-0.

(53) Yao, Y.; Zhang, X.; Mochizuki, K. Solubility of Hydrophobes into Macrocyclic Hosts. *J. Phys. Chem. B* **2022**, *126* (13), 2557–2563. https://doi.org/10.1021/acs.jpcb.2c00728.

(54) Gilson, M. K.; Given, J. A.; Bush, B. L.; McCammon, J. A. The Statistical-Thermodynamic Basis for Computation of Binding Affinities: A Critical Review. *Biophys J* **1997**, *72*, 1047–1069.

(55) Weeks, J. D.; Chandler, D.; Andersen, H. C. Role of Repulsive Forces in Determining the Equilibrium Structure of Simple Liquids. *J. Chem. Phys.* **1971**, *54* (12), 5237–5247. https://doi.org/10.1063/1.1674820.

(56) Jover, J.; Haslam, A. J.; Galindo, A.; Jackson, G.; Müller, E. A. Pseudo Hard-Sphere Potential for Use in Continuous Molecular-Dynamics Simulation of Spherical and Chain Molecules. *J. Chem. Phys.* **2012**, *137* (14), 144505. https://doi.org/10.1063/1.4754275.

(57) Beutler, T. C.; Mark, A. E.; van Schaik, R. C.; Gerber, P. R.; van Gunsteren, W. F. Avoiding Singularities and Numerical Instabilities in Free Energy Calculations Based on Molecular Simulations. *Chem. Phys. Lett.* **1994**, *222* (6), 529–539. https://doi.org/10.1016/0009-2614(94)00397-1.

(58) Matos, I. Q.; Abreu, C. R. A. Evaluation of the SAFT-γ Mie Force Field with Solvation Free Energy Calculations. *Fluid Phase Equilibria* **2019**, *484*, 88–97. https://doi.org/10.1016/j.fluid.2018.11.018.

(59) Shirts, M. R.; Chodera, J. D. Statistically Optimal Analysis of Samples from Multiple Equilibrium States. *J. Chem. Phys.* **2008**, *129* (12), 124105. https://doi.org/10.1063/1.2978177.

(60) Floris, F. M. Modeling the Cavitation Free Energy. *J. Phys. Chem. B* **2005**, *109* (50), 24061–24070. https://doi.org/10.1021/jp053457+.

(61) Jorgensen, W. L.; Chandrasekhar, J.; Madura, J. D.; Impey, R. W.; Klein, M. L. Comparison of Simple Potential Functions for Simulating Liquid Water. *J. Chem. Phys.* **1983**, *79* (2), 926–935. https://doi.org/10.1063/1.445869.

(62) Kumar, S.; Rosenberg, J. M.; Bouzida, D.; Swendsen, R. H.; Kollman, P. A. THE Weighted Histogram Analysis Method for Free-Energy Calculations on Biomolecules. I. The Method. *J. Comput. Chem.* **1992**, *13* (8), 1011–1021. https://doi.org/10.1002/jcc.540130812.

(63) Jakalian, A.; Bush, B. L.; Jack, D. B.; Bayly, C. I. Fast, Efficient Generation of High-Quality Atomic Charges. AM1-BCC Model: I. Method. *J. Comput. Chem.* **2000**, *21* (2), 132–146. https://doi.org/10.1002/(SICI)1096-987X(20000130)21:2<132::AID-JCC5>3.0.CO;2-P.

(64) Jakalian, A.; Jack, D. B.; Bayly, C. I. Fast, Efficient Generation of High-Quality Atomic Charges. AM1-BCC Model: II. Parameterization and Validation. *J. Comput. Chem.* **2002**, *23* (16), 1623–1641. https://doi.org/10.1002/jcc.10128.

(65) Case, D. A.; Aktulga, H. M.; Belfon, K.; Ben-Shalom, I. Y.; Berryman, J. T.; Brozell, S. R.; Cerutti, D. S.; Cheatham, T. E., III; Cisneros, G. A.; Cruzeiro, V. W. D.; Darden, T. A.; Duke, R. E.; Giambasu, G.; Gilson, M. K.; Gohlke, H.; Goetz, A. W.; Harris, R.; Izadi, S.; Izmailov, S. A.; Kasavajhala, K.; Kaymak, M. C.; King, E.; Kovalenko, A.; Kurtzman, T.; Lee, T. S.; LeGrand, S.; Li, P.; Lin, C.; Liu, J.; Luchko, T.; Luo, R.; Machado, M.; Man, V.; Manathunga, M.; Merz, K. M.; Miao, Y.; Mikhailovskii, O.; Monard, G.; Nguyen, H.; O'Hearn, K. A.; Onufriev, A.; Pan, F.; Pantano, S.; Qi, R.; Rahnamoun, A.; Roe, D. R.; Roitberg, A.; Sagui, C.; Schott-Verdugo, S.; Shajan, A.; Shen, J.; Simmerling, C. L.; Skrynnikov, N. R.; Smith, J.; Swails, J.; Walker, R. C.; Wang, J.; Wang, J.; Wei, H.; Wolf, R. M.; Wu, X.; Xiong, Y.; Xue, Y.; York, D. M.; Zhao, S.; Kollman, P. Amber 2022, University of California, San Francisco., 2022.

(66) Eastman, P.; Swails, J.; Chodera, J. D.; McGibbon, R. T.; Zhao, Y.; Beauchamp, K. A.; Wang, L.-P.; Simmonett, A. C.; Harrigan, M. P.; Stern, C. D.; Wiewiora, R. P.; Brooks, B. R.; Pande, V. S. OpenMM 7: Rapid Development of High Performance Algorithms for Molecular Dynamics. *PLOS Comput. Biol.* **2017**, *13* (7), e1005659. https://doi.org/10.1371/journal.pcbi.1005659.

(67) Darden, T.; York, D.; Pedersen, L. Particle Mesh Ewald: An *N*·log(*N*) Method for Ewald Sums in Large Systems. *J. Chem. Phys.* **1993**, *98* (12), 10089–10092. https://doi.org/10.1063/1.464397.

(68) Essmann, U.; Perera, L.; Berkowitz, M. L.; Darden, T.; Lee, H.; Pedersen, L. G. A Smooth Particle Mesh Ewald Method. *J. Chem. Phys.* **1995**, *103* (19), 8577–8593. https://doi.org/10.1063/1.470117.

(69) Izaguirre, J. A.; Sweet, C. R.; Pande, V. S. Multiscale Dynamics of Macromolecules Using Normal Mode Langevin. In *Biocomputing 2010*; WORLD SCIENTIFIC, 2009; pp 240–251. https://doi.org/10.1142/9789814295291_0026.

(70) Chow, K.-H.; Ferguson, D. M. Isothermal-Isobaric Molecular Dynamics Simulations with Monte Carlo Volume Sampling. *Comput. Phys. Commun.* **1995**, *91* (1–3), 283–289. https://doi.org/10.1016/0010-4655(95)00059-O.

(71) Åqvist, J.; Wennerström, P.; Nervall, M.; Bjelic, S.; Brandsdal, B. O. Molecular Dynamics Simulations of Water and Biomolecules with a Monte Carlo Constant Pressure Algorithm. *Chem. Phys. Lett.* **2004**, *384* (4–6), 288–294. https://doi.org/10.1016/j.cplett.2003.12.039.

(72) Marquez, C.; Nau, W. M. Polarizabilities Inside Molecular Containers. *Angew. Chem. Int. Ed.* **2001**, *40* (23), 4387–4390. https://doi.org/10.1002/1521-3773(20011203)40:23<4387::AID-ANIE4387>3.0.CO;2-H.

(73) Ben-Naim, A. Inversion of the Hydrophobic/Hydrophilic Paradigm Demystifies the Protein Folding and Self-Assembly of Problems. *Int. J. Phys.* **2013**, *1* (3), 66–71. https://doi.org/10.12691/ijp-1-3-2.

(74) Widom, B. Structure of Interfaces from Uniformity of the Chemical Potential. *J. Stat. Phys.* **1978**, *19* (6), 563–574. https://doi.org/10.1007/BF01011768.

(75) Frenkel, D.; Smit, B. *Understanding Molecular Simulation: From Algorithms to Applications*, 2nd ed.; Academic Press, 2001.
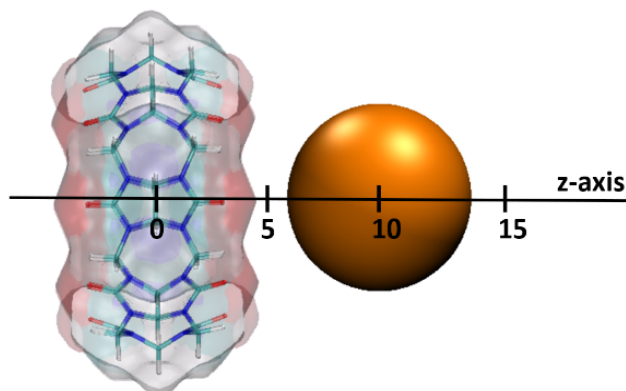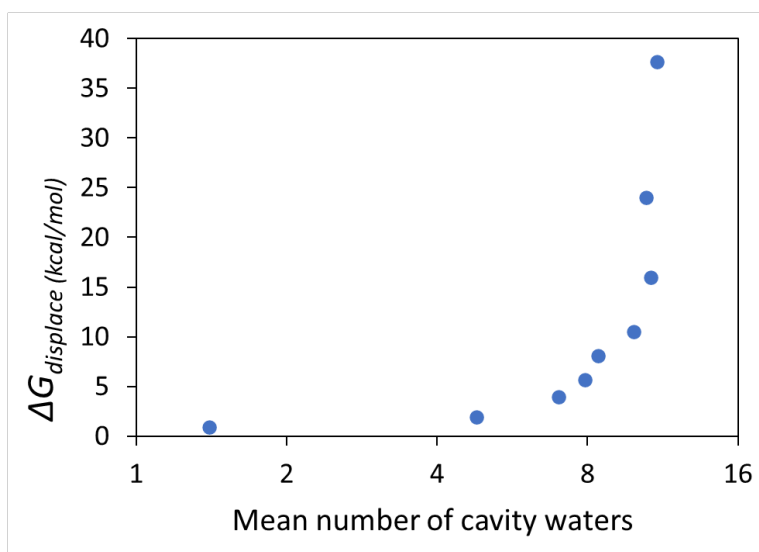
Extended Data
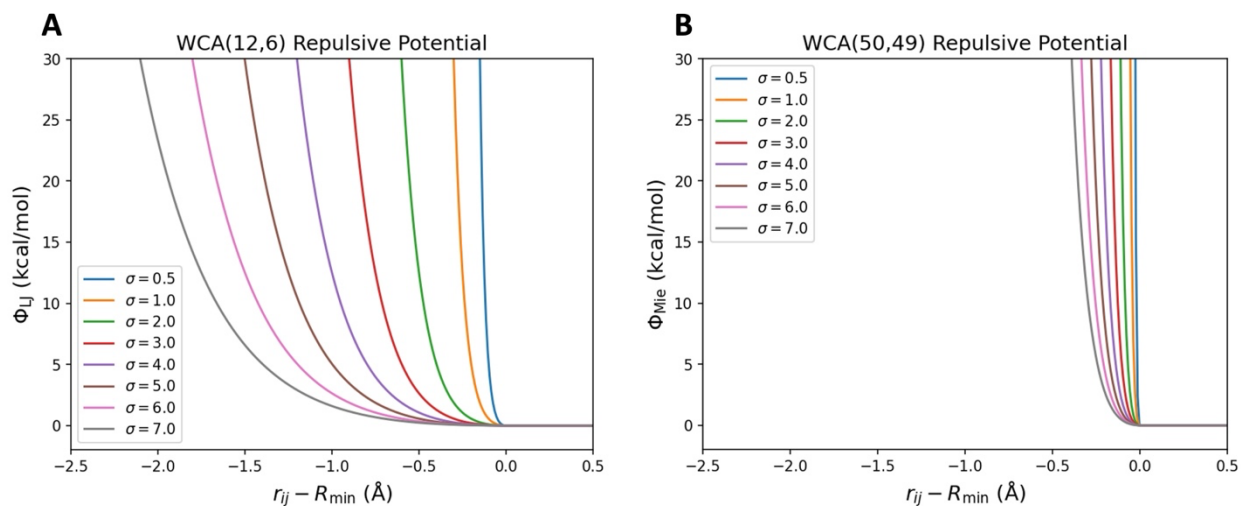
Extended Data Figure S1. Graphs of candidate pseudo-hard sphere potentials plotted relative to the quantity $r_{ij} - R_{\min}$ (shifted r_{ij}) to better superpose the curves for the cut-and-shifted WCA (A) 12-6 LJ potential and (B) 50-49 Mie potential. The σ values are reported in units of Å.
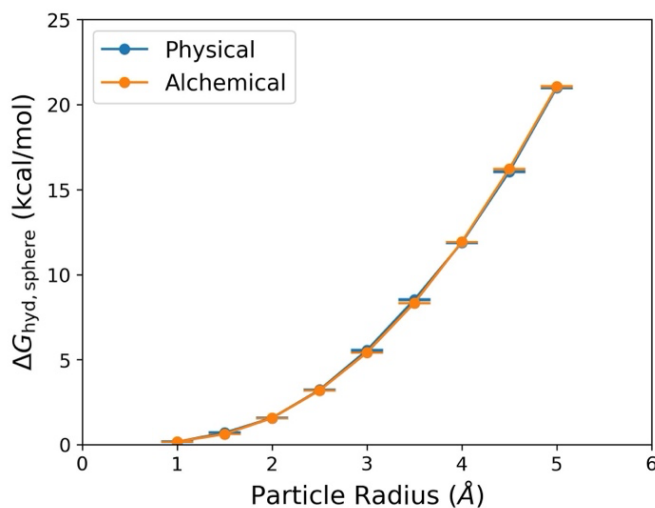
Extended Data Figure S2. Comparison of the hydration free energy (HFE) of pseudo hard-sphere particles (PHSP) of various radii (R_{particle}), computed with the physical path-based and alchemical methods.

Extended Data Figure S3. Diagram of PHSP guest (orange) at z = 10 Å while being inserted into the CB8 binding cavity (sticks and transparent surface).

Extended Data Figure S4. Free energy of water displacement as a function of the mean number of cavity waters, here plotted on logarithmic horizontal axis. The data are the same as those plotted in Figure 6.

Extended Data Table S1. The change in the free energy of hydration of the pseudo-hard-sphere particle, computed with the physical and alchemical methods, for different particle sizes.

R_{particle} (Å)	$\Delta G_{\text{hyd,sphere}}^{\text{Physical}}$ (kcal/mol)	$\Delta G_{\text{hyd,sphere}}^{\text{Alchemical}}$ (kcal/mol)
1.0	0.17 ± 0.03	0.17 ± 0.00
1.5	0.70 ± 0.04	0.62 ± 0.00
2.0	1.57 ± 0.04	1.56 ± 0.01
2.5	3.22 ± 0.04	$3.18 + 0.01$
3.0	5.55 ± 0.05	5.41 ± 0.01
3.5	8.53 ± 0.04	8.33 ± 0.02
4.0	11.88 ± 0.04	11.92 ± 0.02
4.5	16.05 ± 0.04	16.21 ± 0.03
5.0	20.99 ± 0.04	21.07 ± 0.03